Numerical noise generation in modelled bearing vibration signals

Sarabjeet SINGH[1]; Carl Q. HOWARD[2]; Colin H. HANSEN[3]; Uwe KÖPKE[4]

[1,2,3]School of Mechanical Engineering, The University of Adelaide, South Australia 5005 Australia

[4]Trackside Intelligence Pty. Ltd., 17–19 King William St, Kent Town SA 5067

ABSTRACT

A two-dimensional (2-D) explicit dynamics finite element (FE) model of a rolling element bearing was solved using a commercial FE software package, LS-DYNA. It was found that the modelled bearing vibration signals contain a significant amount of numerical noise. This paper provides an explanation of the physical mechanism by which the numerical noise is generated. The noise frequencies were analytically estimated and filtered out to achieve comparatively clean vibration signals and rolling element-to-raceway contact forces.

Keywords: Rolling element bearing, Vibrations, LS-DYNA I-INCE Classification of Subjects Number(s): 11.1.1, 75.3

1. INTRODUCTION

A 2-D explicit dynamics, non-linear, FE model of a rolling element bearing was build and solved using a commercially available FE software package, LS-DYNA (1). The model comprises the following components: an outer ring, an inner ring, a cage retaining a total of twenty-four rolling elements, and an adapter that distributes a (radial) load to the outer ring, which is also transmitted to the inner ring through the rolling elements. In addition to the vibration response, contact forces between the rolling elements and raceways of the bearing were also modelled. A significant amount of numerical noise was observed in the FE simulation results, and a hypothesis was developed to explain the cause of the noise. The numerical noise frequencies were analytically estimated and filtered out to achieve comparatively clean vibration signals and contact forces. Favourable comparison between the analytical and numerical noise frequencies justifies the proposed hypothesis.

2. FINITE ELEMENT MODEL OF A ROLLING ELEMENT BEARING

2.1 Description of the model

The dimensions of the aforementioned components of the bearing are shown in Table 1. 2-D shell elements were used to model the bearing as a solid structure. A 2-D element is defined by four nodes having 2-degrees-of-freedom at each node: translations in the nodal x- and y-directions. The shell elements were modelled as plane strain elements (1, pp. 3.25–3.30). The components of the bearing were modelled using the material properties of steel of density $\rho = 7850\,\mathrm{kg/m^3}$, modulus of elasticity $E = 200\,\mathrm{GPa}$, and Poisson's ratio $\nu = 0.3$. The isotropic elastic material model was chosen for the current analysis.

The bearing was modelled with a localised rectangular-shaped defect that was located centrally at the top on the outer raceway. The dimensions of the defect were: circumferential length $L_d = 10\,\mathrm{mm}$ and height (or depth) $H_d = 0.2\,\mathrm{mm}$.

2.2 Discretisation of the model

The discretisation of a model into nodes and elements is an important step in an FE analysis as the accuracy of the results depends on the quality of the mesh, and size and aspect ratio of the elements. Elements with poor aspect ratio can lead to severe (elemental) distortion or *hourglassing* (1, pp. 3.4–3.16, 7.6–7.9). All the components within the rolling element bearing model were meshed using quadrilateral elements, except for the rolling elements, which due to their geometry, could not be meshed with the quadrilateral elements. Consequently, they were meshed with a mixture of quadrilateral and triangular elements. An element mesh

[1]sarabjeet.singh@adelaide.edu.au
[2]carl.howard@adelaide.edu.au
[3]colin.hansen@adelaide.edu.au
[4]uwek@trackiq.com.au

Table 1 – Dimensions of the components within the FE model of the bearing.

Component name	Description and dimensions (mm)			
Outer ring	outer race diameter	$D_o = 200$	thickness	$h_o = 10$
Inner ring	inner race diameter	$D_i = 163.96$	thickness	$h_i = 10$
Cage	outer diameter	$D_c = 196$	thickness	$h_c = 4$
Rolling element	diameter	$D_r = 18$	total number	$N_r = 24$
Adapter	width	$w_a = 160$	height (central)	$H_a = 40$

size of 0.5 mm was used to uniformly discretise the model. The reason for choosing such a small element mesh size is to achieve compliance of the FE simulation results with the following two conditions, so as to simulate a real-scenario of a bearing operation:

1. the surfaces of the bearing raceways and rolling elements, which are under the influence of load zone (2, pp. 234–237), should be in contact at all times during the simulation, and
2. the rolling elements should predominantly roll and not slide during the simulation.

Fulfilment of the first condition is necessary to achieve the correct load distribution on the rolling elements as per the analytical static solution (3). Accomplishment of the second condition is necessary to accurately acquire the rotational speed of the rolling elements (cage) ω_c, which would eventually result in the correct prediction of the bearing kinematics; that is, the outer raceway defect frequency f_{bpo} for the current simulation. The chosen element mesh size of 0.5 mm corresponds to 97 elements-per-wavelength (EPW) (at 40 kHz), which is nearly 5 times the recommended EPW criterion of 20 EPW for a transient dynamic structural analysis (4, Chapter 5). A discussion on the procedure of estimating the EPW value based on the bending wave speed of the outer ring of the bearing is explained in Ref (5).

Figure 1 shows the meshed FE model of the rolling element bearing annotated with the names of the components. The geometrical rectangular defect located centrally at the top of the outer raceway, which cannot be seen in Figure 1a, is shown in Figure 1b for clarity. The centre of the rolling element located immediately to the left-hand side of the defect is offset by at 4° from the *y*-axis; the rolling elements within the model are spaced 15° apart.

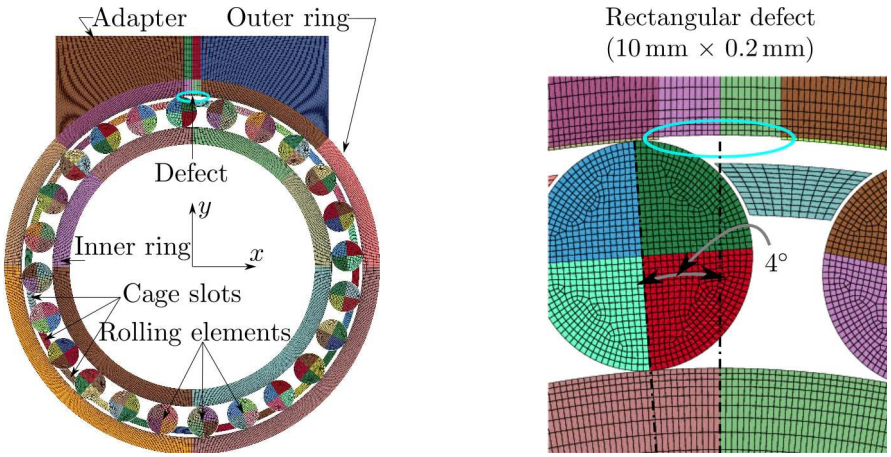

Figure 1 – Images of the 2-D FE model of the defective rolling element bearing: (a) the meshed FE bearing model along with the adapter, and (b) a partially zoomed version of Figure 1a, showing the 1-element deep rectangular defect on the outer raceway, highlighted using the ellipse; the centre of the rolling element to the left-hand side of the defect is offset by 4° from the *y*-axis.

2.3 Boundary conditions and loads

The following boundary conditions were applied to the FE model of the rolling element bearing in order to simulate the real-time operation of a bearing.

- A radial load W of 50 kN on the top edge of the adapter in the downward (negative) global cartesian *y*-direction was applied so as to radially load the bearing.
- The inner ring was constantly rotated with a uniform angular velocity ω_s of 500 revolutions per minute

in a clockwise direction.

- The top edge of the adapter was translationally constrained in the global cartesian *x*-direction, and a frictional contact with a high coefficient of friction $\mu_{a-o} = 0.1$ between the outer ring and adapter was implemented. This was done to prevent the outer ring from rotation during the simulation. It should be noted that no direct constraints could be applied to the outer ring as this would result in over-constraining its translations and vibration response, consequently causing an incorrect load distribution on the rolling elements.
- A frictional contact with a low coefficient of friction $\mu = 0.005$ was defined for the following contact interfaces: rolling elements–outer ring, rolling elements–inner ring, and rolling elements–cage. In addition to modelling the surface-to-surface contact at the aforementioned interfaces, the segment-based contact formulation (1, pp. 26.10) was implemented during the numerical simulation.
- A global (mass-weighted) damping of 2% was applied to the model.
- The standard Earth's gravity was also applied to the model.

3. NUMERICALLY MODELLED ACCELERATION TIME-TRACE

The termination time of the numerical simulations was set to 30 milli-seconds (ms). The results, in the form of binary text files, were written at an interval of 0.01 ms, which corresponds to a sampling rate of 100 kHz.

Figure 2 shows the (unfiltered) time-trace of the numerically obtained acceleration a_y (in the global *y*-direction) for a node located on the outer surface of the outer ring. The three consecutive defect-related impulses, evident in the plot, are separated by approximately 0.011 seconds, which corresponds to the outer raceway defect frequency f_{bpo} of 90.91 Hz. The analytical estimation of the nominal BPFO, f_{bpo}, is given by (2, p. 994)

$$f_{\text{bpo}} = \frac{f_s \times N_r}{2}\left(1 - \frac{D_r}{D_p}\cos\alpha\right) \tag{1}$$

where, f_s is the bearing run speed (that is, the rotational speed of shaft or inner ring), N_r is the number of rolling elements, D_r is the rolling element diameter, D_p is the bearing pitch diameter, and α is the contact angle. For the bearing modelled here, the analytical estimate of the BPFO, calculated using Equation (1), is 90.07 Hz, which is 0.9% different from the results of the numerical simulation. The slight difference between the numerical and analytical estimates is because the analytical formula, shown in Equation (1), does not account for the slippage of the rolling elements (6), which was accounted in the explicit FE analysis of the bearing undertaken here.

Close agreement between the numerical and analytical values of the outer raceway defect frequency shows that the FE model has satisfactorily simulated the basic bearing kinematics. However, the acceleration time-trace has a substantial amount of numerical noise, which is explained in the following section.

4. NUMERICAL CONTACT NOISE — AN ARTEFACT OF THE MODEL

It can be observed in Figure 2 that while the instantaneous peak impulsive acceleration levels for the three visible defect-related impacts range from 0 to approximately ± 180 g, the non-impulsive acceleration levels between the impacts are of the order of ± 50 g. In order to seek the frequencies associated with the numerical noise, power spectrum of the numerical acceleration signal, shown in Figure 2, was calculated for a frequency resolution of 3 Hz. The narrow band power spectral density of the numerically modelled acceleration a_y signal is shown in Figure 3. A fundamental tone at 4671 Hz, as indicated in the figure, corresponds to the numerical noise. There is also an indication of the 5^{th} harmonic at approximately 23 kHz in the figure that is associated with the fundamental tone. In addition to the dominant numerical noise at 4671 Hz, another frequency component that was intermittently observed in the numerical acceleration a_y time-trace was 4545 Hz; however, it is not apparent in the power spectrum.

A development and justification of a novel hypothesis for explaining the cause of the numerical noise frequencies are described in the next section.

4.1 Hypothesis for explaining the cause of numerical contact noise

Because the circular rolling elements were discretised into a number of finite elements, the edges of the rolling elements were transformed from circular to multi-point polygons. Figure 4 shows a schematic of a polygonised rolling element. It does not represent an actual size of a rolling element, which is included in the FE model of the rolling element bearing. In the schematic, only a few points, 15, were used to create the polygon for clarity; however, in the FE model, the rolling elements were discretised using the element size of 0.5 mm, which generates a polygon with 113 edges ($= \pi D_r/0.5$), where $D_r = 18$ mm. As they roll during the

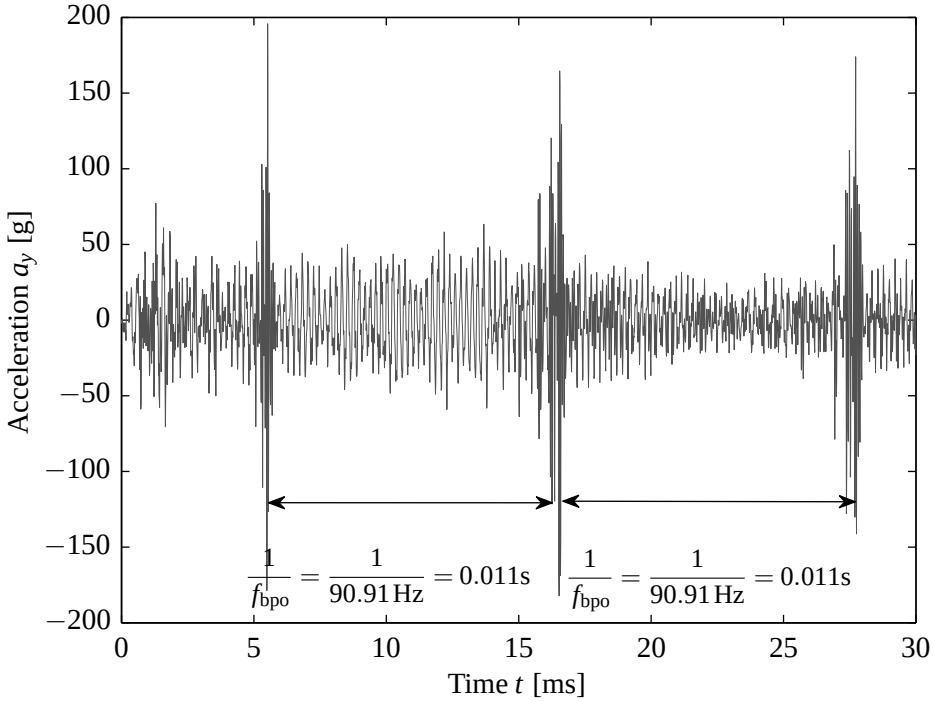

Figure 2 – Numerically modelled, unfiltered, acceleration a_y time-trace for a node located on the outer surface of the outer ring of the FE bearing model for a radial load W of 50 kN and a rotational speed n_s of 500 RPM.

simulation, the *polygonised* rolling elements create small impacts as their points contact the outer and inner raceways. In this case, the frequencies of these impacts would be a function of the element size l_{fe} used to mesh the rolling elements and the rotational velocity of the rolling elements $\omega_c = 2\pi f_c$.

In order to estimate the numerical rolling noise frequency components, a basic equation of motion can be used as follows

$$f_{\text{noise}} = \frac{1}{T_{\text{noise}}} = \frac{2\pi f_c \times D_{\text{race}}}{2l_{\text{fe}}} \tag{2}$$

where, l_{fe} is the distance between two nodes on the (polygonised) edge of the rolling elements within the FE model (mesh element size, 0.5 mm), ω_c is the angular velocity with which the rolling elements roll during the simulation, and D_{race} can either be the diameter of the outer raceway ($D_o = 200$ mm) or inner raceway ($D_i = 163.96$ mm) which contact the rolling elements. Solving Equation (2) for the values of D_{race} as 200 mm and 163.96 mm, the rolling contact noise frequencies equal 4712 Hz and 3864 Hz, respectively. From now onwards, these frequencies will be referred to as the '*rolling element-to-outer raceway*' f^o_{noise}, and '*rolling element-to-inner raceway*' f^i_{noise} rolling contact noise frequencies, respectively.

The analytically estimated rolling element-to-outer raceway rolling contact noise frequency f^o_{noise}, 4712 Hz, differs from one of the noisy frequency components, 4671 Hz, observed in the numerical acceleration signal by 0.8% only. This indicates that the presence of the numerical noise at 4671 Hz is highly likely due to the interaction of the rolling elements with the outer raceway. The slight difference between the analytical and numerical noise frequency estimates is a result of the rolling elements not following a pure rolling movement during the simulation, indicating a small amount of slip.

Another reason for the difference between the analytical and numerical estimations of the rolling element-to-outer raceway rolling contact noise frequency f^o_{noise} is associated with the interaction between the rolling elements and corresponding cage slots. It was found that at certain instances, the rolling elements were drive (pushed) by the cage slots that consequently results in slipping of rolling elements.

4.2 Beating phenomenon

There is a difference of approximately 17% between the other intermittent numerical noise frequency, 4545 Hz, and the analytically estimated rolling element-to-inner raceway rolling contact noise frequency f^i_{noise}, 3864 Hz. As the difference is significant, the analytical and numerical noise frequencies cannot be related. Therefore, the concept of beating (7, p. 45) was applied to explain the occasional presence of the 4545 Hz noise frequency component found in the numerical acceleration results.

As mentioned earlier, the *polygonised* edges of the rolling elements create small impacts with outer and inner raceways as they roll during the simulation. The interaction of the rolling elements with the raceways

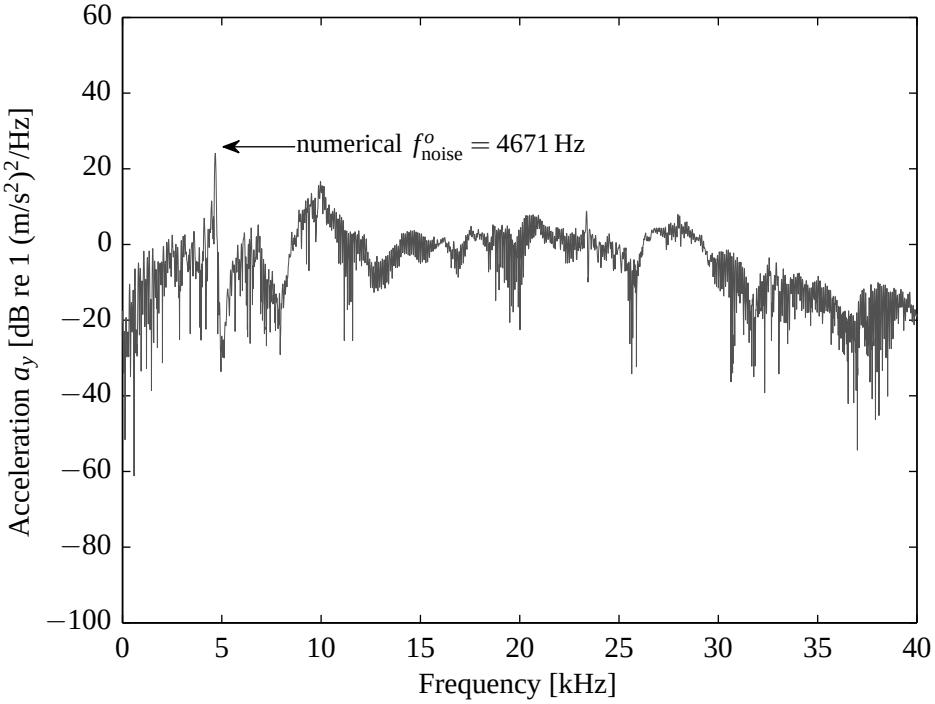

Figure 3 – Power spectral density of the nodal acceleration a_y time-trace shown in Figure 2, highlighting one of the dominant numerical noise frequencies, $f^o_{\text{noise}} = 4671$ Hz observed in the simulation results.

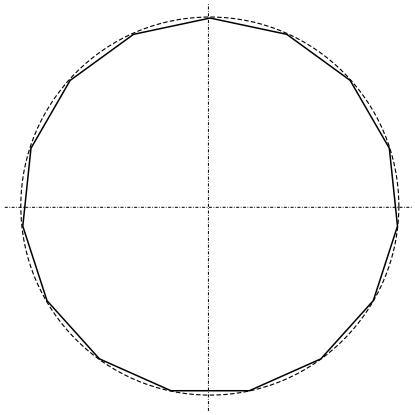

Figure 4 – A schematic of a polygonised rolling element having 15 edges or points (not to scale).

would result in the generation of two sinusoidal waves with a slight difference between their carrier frequencies. The amplitude of the sinusoidal waves would also slightly differ from each other. For the purpose of verifying the aforementioned hypothesis, and demonstrating the beating effect, the sum of two interfering sinusoidal waves is as follows

$$A(t) = A_1 \cos(2\pi f^o_{\text{noise}} t) + A_2 \cos(2\pi f^i_{\text{noise}} t + \phi) \tag{3}$$

where, the amplitudes, $A_1 = A_2 = 1$, t is the time vector, ϕ is the phase shift, and f^o_{noise} and f^i_{noise} are the analytically estimated noise frequencies using Equation (2).

Figure 5a shows the resultant sinusoidal wave, and the same wave along with its envelope, zoomed from 10 ms to 15 ms for clarity, is shown in Figure 5b. The time separation of the two consecutive peaks, whose data cursors are shown in Figure 5b, corresponds to 4545 Hz. This frequency exactly matches the other noise frequency component occasionally observed in the numerically modelled acceleration results. From now onwards, this frequency will be referred to as the *beating noise frequency*, and represented as f^{i-o}_{noise}.

The beating effect can also be clearly observed in Figure 2 between the first two defect-related impulses from approximately 5 ms to 16 ms, but not as clearly between the second and third impulse from approximately 17 ms to 28 ms. One potential reason for not having a clear beating effect is the slippage of the rolling elements which eventually results in no tonal component at the beating noise frequency f^{i-o}_{noise}, in contrast to

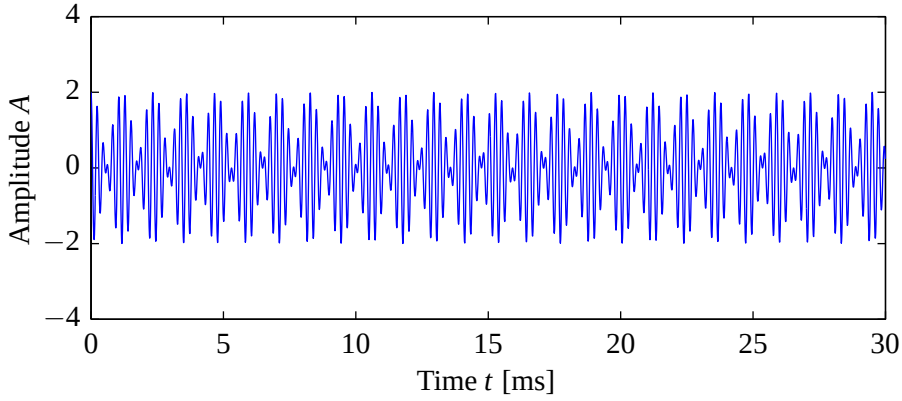

(a) The resultant sinusoidal wave.

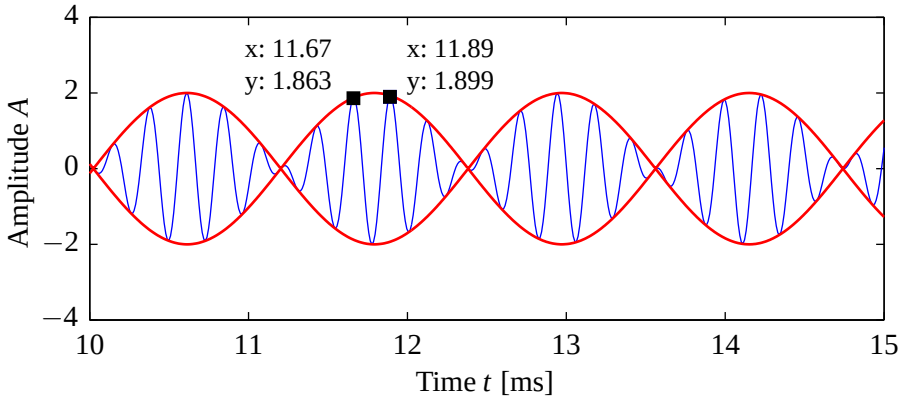

(b) The sinusoidal wave in Figure 5a along with its envelope zoomed for clarity.

Figure 5 – Demonstration of the beating effect due to the interference of two sinusoidal waves at the two analytically estimated noise frequencies $f^{o}_{\text{noise}} = 4712$ Hz and $f^{i}_{\text{noise}} = 3864$ Hz.

the strong fundamental tone at the rolling element-to-outer raceway noise frequency f^{o}_{noise}, as shown in the power spectrum of the acceleration signal in Figure 3. Another reason for there being no tonal component at 4545 Hz could be because the acceleration signal was extracted at a node located on the outer ring of the bearing. In other words, the nodal results on the outer ring are significantly influenced by the interaction of the rolling elements and outer raceway, but comparatively less by the rolling elements-to-inner raceway contact interaction.

The numerical acceleration signal was notch filtered to eliminate the rolling element-to-outer raceway rolling contact noise frequency f^{o}_{noise} of 4671 Hz using a second-order infinite impulse response filter having a quality factor Q of 15. The notch filtered acceleration time-trace is shown in Figure 6. For comparison, the unfiltered acceleration results from Figure 2 are also plotted along with the notch filtered results using a gray-coloured, dashed line. The performance of the filter is evident in Figure 6; the instantaneous levels of the non-impulsive acceleration signals, which prior to the application of the filter ranged between approximately ± 50 g, were reduced to approximately ± 20 g after filtering the dominant rolling element-to-outer raceway rolling contact noise frequency f^{o}_{noise}. However, there is still some residual noise. It is likely that the remaining noise is due to the sliding (slippage) of the rolling elements as a result of their interaction with the cage slots in addition to the inherent adaptive time-stepping variations (1). These noise frequencies are stochastic, and therefore, could not be estimated and filtered without affecting the vibration response of the bearing.

The power spectrum of the unfiltered (Figure 3) and notch filtered acceleration a_y time-traces are compared in Figure 7. In order to clearly see the difference between the two power spectra, the results in Figure 7a are zoomed from 4–6 kHz, and the corresponding plots are shown in Figure 7b. It can be seen that the tone at the numerical rolling element-to-outer raceway rolling contact noise frequency f^{o}_{noise} has been attenuated by approximately 25 dB without affecting the majority of the response. However, the power spectrum at the frequencies within the filter bandwidth is affected slightly. In contrast to the primarily attenuated sharp fundamental noise tone at $f^{o}_{\text{noise}} = 4671$ Hz, slight attenuation (by 4 dB) of the comparatively weak tone at the beating noise frequency $f^{i-o}_{\text{noise}} = 4545$ Hz can also be seen as indicated in Figure 7b.

In summary, it can be concluded that the introduction of noise in the simulation results is an artefact of

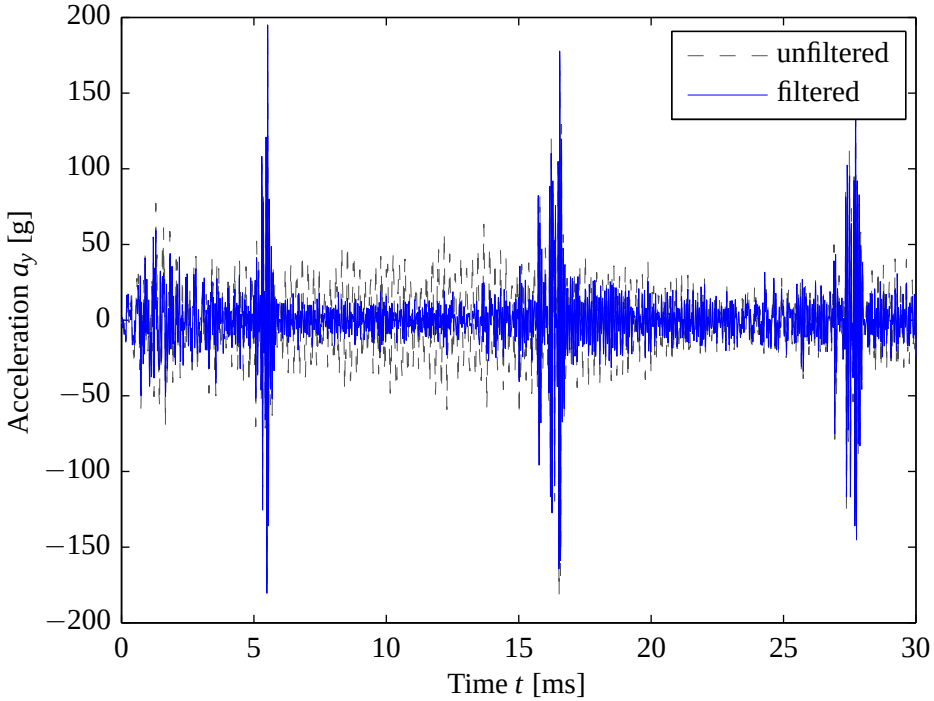

Figure 6 – Effect of filtering out the rolling element-to-outer raceway noise frequency $f^o_{\text{noise}} = 4671$ Hz on the numerically modelled acceleration a_y time-trace shown in Figure 2.

the numerical modelling. A favourable agreement between the numerical and analytical rolling contact noise frequencies justifies the proposed hypothesis for explaining the cause of numerical contact noise observed in the modelled acceleration results.

5. NUMERICALLY MODELLED CONTACT FORCES

For the FE model of the defective rolling element bearing, Figure 8 shows the numerically modelled, unfiltered and notch filtered, vertical F_y contact forces between the outer raceway and three rolling elements, which traversed through the outer raceway defect during the numerical simulation.

The contact forces also contained the numerical noise at the rolling element-to-outer raceway rolling contact noise frequency $f^o_{noise} = 4671$ Hz. Similar to acceleration time-trace, the numerically modelled rolling element-to-outer raceway contact forces were also notch filtered. From the results in Figure 8, it can be seen that the numerical noise in the contact forces was significantly reduced as a result of filtering. Also indicated in the figure are four events, namely events #1 to #4. These events correspond to the variations in the numerically modelled contact forces as the rolling elements traverse through the outer raceway defect. Events #1 is the de-stressing or unloading of the rolling elements as they enter into the defect, event #2 is the impact of the rolling elements with the defcetive surface of the outer raceway, event #3 is the load compenstation by other rolling elements as a rolling element loses its load while traversing the defect, and event #4 is the re-stressing of the rolling elements between the outer and inner raceway in the vicinity of the end of the defect due to which defect-related impulsive acceleration signals are generated, which are observed in practice and used for bearing diagnosis. A detailed discussion on these events along with the correlation of the contact forces with acceleration results is provided in references (5, 8).

From the results presented in Figures 7 and 8, it is evident that the notch filtered acceleration and contact forces are comparatively cleaner than the corresponding unfiltered results.

6. CONCLUSIONS

A hypothesis was developed to explain the cause of numerical noise generated in the explicit FE simulation results due to the rolling contact of the ploygonised rolling elements and raceways of a rolling element bearing. The noise frequencies were analytically estimated and compared to those observed in the simulation results. A favourable comparison between the numerical and analytical estimates of the noise frequencies justifies the proposed hypothesis. The numerical noise was filtered out from the acceleration and contact forces, and a reasonably cleaner results were achieved.

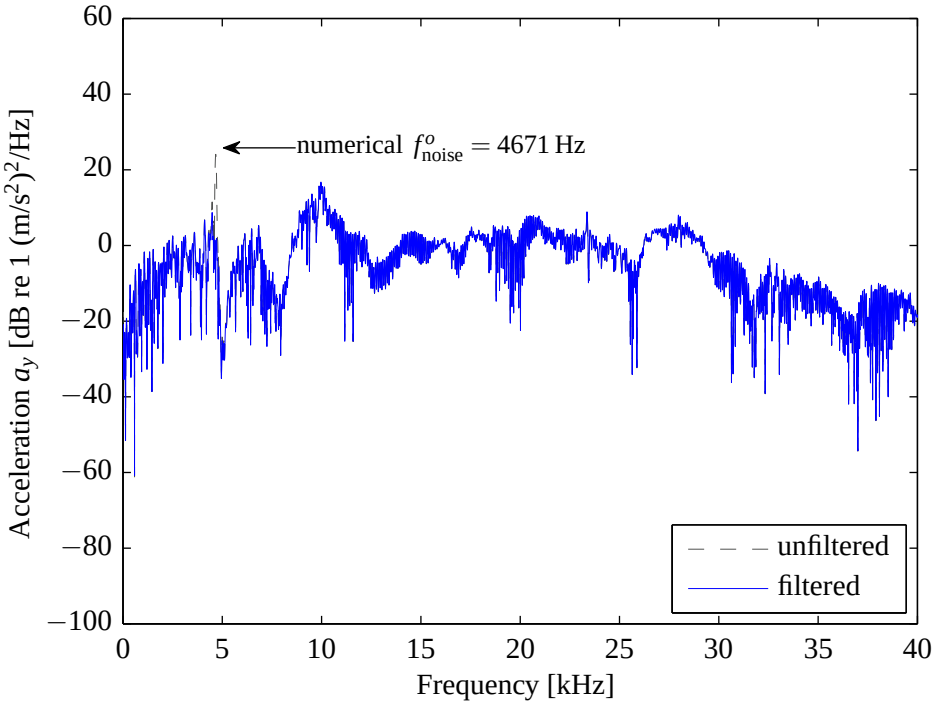

(a) Power spectral densities of the unfiltered and notch filtered acceleration a_y time-traces, highlighting the tonal noise at $f^{o}_{\text{noise}} = 4671$ Hz for the unfiltered time-trace.

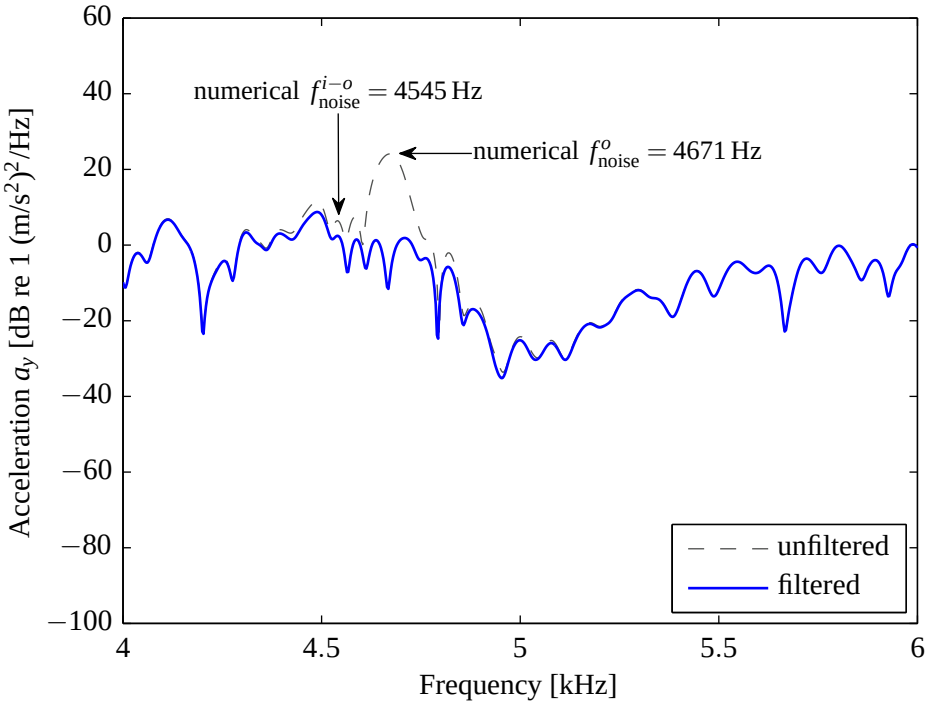

(b) Comparison of the power spectral densities, shown in Figure 7a, on a zoomed frequency scale of 4–6 kHz, highlighting the attenuation of the tonal noise by 25 dB after filtering.

Figure 7 – Power spectrum of the numerically modelled, unfiltered and notch filtered, acceleration a_y time-traces, shown in Figure 6.

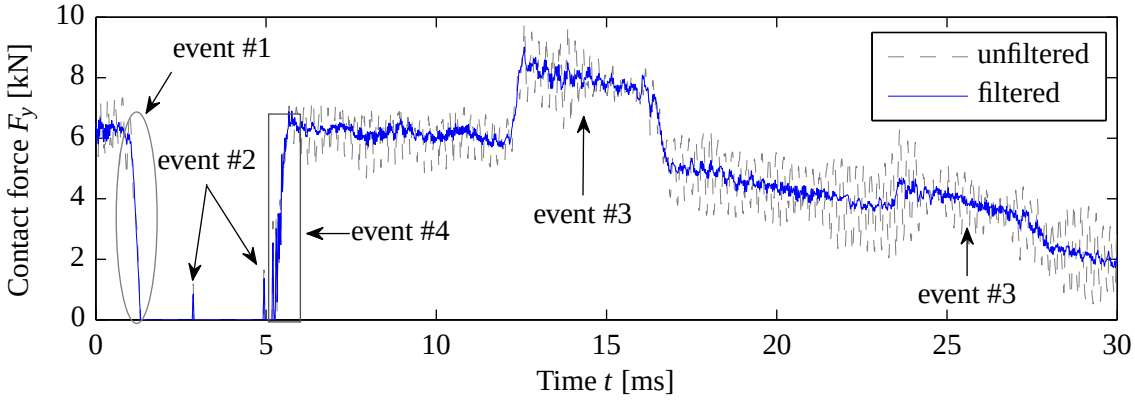

(a) Vertical contact force between the first rolling element and outer raceway.

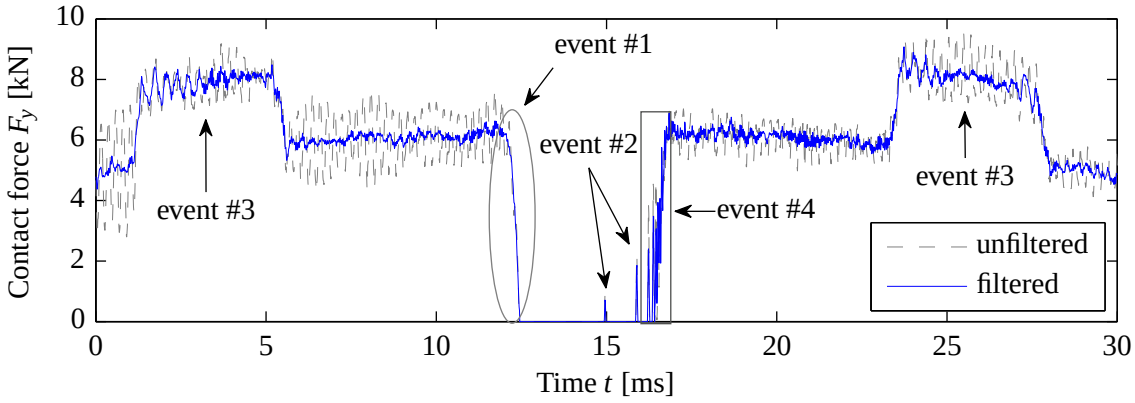

(b) Vertical contact force between the second rolling element and outer raceway.

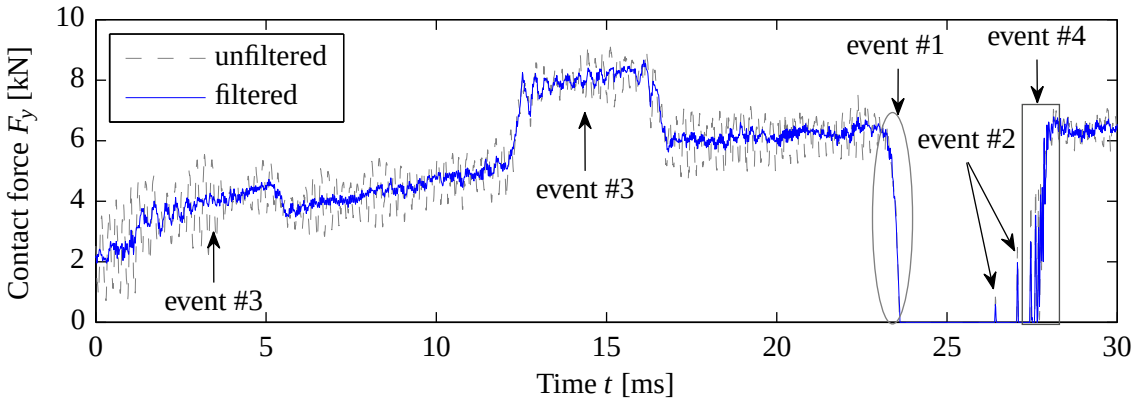

(c) Vertical contact force between the third rolling element and outer raceway.

Figure 8 – Numerically modelled, unfiltered and notch filtered, vertical rolling element-to-outer raceway contact forces F_y as three rolling elements traverse through the outer raceway defect for a radial load W of 50 kN and rotational speed n_s of 500 RPM.

ACKNOWLEDGEMENTS

This work was conducted as a part of ARC Linkage funded project LP110100529.

REFERENCES

1. Hallquist JO. LS-DYNA Theory Manual; 2006.
2. Harris TA. Rolling Bearing Analysis. Fourth ed. John Wiley & Sons; 2001.
3. Petersen D, Howard C, Sawalhi N, Ahmadi A, Singh S. Analysis of bearing stiffness variations, contact forces and vibrations in radially loaded double row ball bearings with raceway defects. Mechanical Systems and Signal Processing. 2014;50–51:139–160.
4. ANSYS, Release 14.5, Help System, Structural Anslysis Guide, SAS IP, Inc.; 2013.
5. Singh S, Köpke U, Howard C, Petersen D. Analyses of contact forces and vibration response for a defective rolling element bearing using an explicit dynamics finite element model. Journal of Sound and Vibration. 2014;333(21):5356–5377.
6. Randall RB, Antoni J. Rolling element bearing diagnostics — A tutorial. Mechanical Systems and Signal Processing. 2011;25(2):485–520.
7. Bies D, Hansen C. Engineering Noise Control: Theory and Practice. Fourth ed. Taylor & Francis; 2009.
8. Singh S, Köpke U, Howard C, Petersen D, Rennison D. Impact generating mechanisms in damaged rolling element bearings. In: Proceedings of Acoustics. Paper number 106. Victor Harbor, South Australia, Australia: Australian Acoustical Society; 2013. .